Investigating Fracture Properties of The Additively Manufactured PLA Using Sub-Size Specimens

Sarinova Simandjuntak (sarinova.simandjuntak@port.ac.uk)
University of Portsmouth https://orcid.org/0000-0003-3167-6882

Chulin Jiang
University of Portsmouth Department of Mechanical and Design Engineering: University of Portsmouth School of Engineering

Tobias Kathke
University of Portsmouth

David Sanders
University of Portsmouth Department of Mechanical and Design Engineering: University of Portsmouth School of Engineering

Jiye Chen
University of Portsmouth School of Earth and Environmental Sciences

Nils Bausch
University of Portsmouth Faculty of Technology

Research Article

Keywords: Strain Energy Release Rate, Fracture Toughness, PLA, Additive Manufacturing, Sub-size, Impact test

Posted Date: February 25th, 2021

DOI: https://doi.org/10.21203/rs.3.rs-210665/v1

International Journal of Advanced Manufacturing Technology:

Declarations:

Compliance with Ethical Standards
Authors would like to confirm that principles of ethical and professional conduct have been followed throughout the research and the writing of the paper.

Research involving human participants and/or animals
There is no part of the research or work that involved human participants and/or animals

Informed consent
The research/work did not involve disclosure of personal information.

Funding (information that explains whether and by whom the research was supported)
The work presented came from the master and PhD research undertaken at the School of Mechanical and Design Engineering, University of Portsmouth.

Conflicts of interest/Competing interests (include appropriate disclosures)
There is no conflict of interests that are directly or indirectly related to the work submitted for publication.

Availability of data and material (data transparency)
Yes, data and material for transparency will be made available.

Code availability (software application or custom code)
N/A

Authors' contributions (optional: please review the submission guidelines from the journal whether statements are mandatory)
All authors contributed to the study conception and design. Material preparation, data collection and analysis were performed by Sarinova Simandjuntak, Tobias Kathke and Chulin Jiang. The first draft of the manuscript was written by Sarinova Simandjuntak and all authors commented on previous versions of the manuscript. All authors read and approved the final manuscript.

ORCID No:

- Sarinova Simandjuntak: 0000-0003-3167-6882
- Chulin Jiang: N.A
- Tobias Kathke: N.A
- David Sanders: 0000-0002-4359-6743
- Jiye Chen: 0000-0002-2817-5211
- Nils Bausch: 0000-0001-9219-6052

Investigating Fracture Properties of the Additively Manufactured PLA using Sub-Size Specimens

Sarinova Simandjuntak[1], Chulin Jiang[1], Tobias Kathke[1], David Sanders[1], Jiye Chen[2], Nils Bausch[3]
[1]School of Mechanical and Design Engineering, University of Portsmouth, PO1 3DJ, UK;
[2]School of Civil Engineering and Surveying, University of Portsmouth, PO1 3AH
[3]School of Energy and Electronic engineering, University of Portsmouth, PO1 3DJ

Author correspondence: Sarinova.simandjuntak@port.ac.uk

Abstract
In the absence of an acceptable test standard for determining fracture properties of a single edge notched sub-size non-metallic (plastic) specimen, the test method's viability of the ASTM-5045's energy approach and the Roberts and Newton solution for Charpy V-Notch (CVN) impact testing was investigated. The strain energy release rate (SERR) and fracture toughness were determined by subjecting the sub-size specimens of additively manufactured Polylactic Acid (PLA) to a three-point flexural and a CVN impact testing. A Fused Deposition Modelling (FDM) technique was adapted to manufacture thin specimens by sequentially layering a 100μm thick raster in (-45/45)° and (0/90)° orientation. The toughness values of the flexural specimens increase with the number of layers (specimen thickness) and are clearly influenced by the layer orientation. Thicker CVN impact test specimens, however, resulted in relatively lower toughness values. This was due to a reduction of constraints for plane strain conditions that the existing impact test standard/procedure considered. When compared with the impact testing method, the flexural testing using the energy approach demonstrates a better capability to capture the effect of an increase in the energy absorbed for the air gaps to plastically deform and for the delamination to take place in the sub-size specimens. The X-Ray Tomographic images of the flexural test specimens confirmed the presence of air gaps where the onset of the cracking and delamination were observed, whilst the micrographic images revealed mode I intra-laminar fracture for all test specimens.

Key words
Strain Energy Release Rate, Fracture Toughness, PLA, Additive Manufacturing, Sub-size, Impact test.

1. Background

Biodegradable PLA (Polylactic Acid), which is a vegetable-based plastic, has had an increased interest from many industries and sectors, such as medical, textile and food industries. PLA has however restricted structural applications given its biological susceptibility and brittleness. PLA's poor toughness limits its application that requires plastic deformation at higher stress levels. Although in comparison to traditional polymers like polypropylene, polystyrene, and polyurethane, PLA has relatively higher

stiffness ratio, tensile and flexural strengths (Auras et al., 2004) (Farah et al., 2016). PLA is now a common material used for filaments in rapid prototyping and additive manufacturing (AM), of which Fused Deposition Modelling (FDM) is one of the AM techniques. The process involves layering a thin, continuous filament made of a thermoplastic material to form objects or component parts by translating a computer aided design (CAD) model or a 3D scanned object (Diegel, 2014) (Guo and Leu, 2013). Due to the additive layering principle, this manufacturing process can now address different geometries such as lightweight structures (Zhang et al., 2016) (Petrovic et al., 2011) and complex biological structures (Murphy and Atala, 2014) (Chin Ang et al., 2006) (Kalita, 2010) (Singh et al., 2016).

The potential of the AM processes available today can be fully exploited when the control of manufacturing processes and the impact of the FDM parameters is understood better. These parameters are for example: nozzle shape and size, as-built and layer orientation, infill density and pattern, raster thickness, air gap, feed rate, and print velocities (Sood et al., n.d.) (Lanzotti et al., 2015). This means that manufacturing reproducible products with close tolerances and in a time and cost-efficient manner can be challenging. The tolerances relate not only to the geometric dimensions but also to the intrinsic mechanical characteristics and the surface quality. The quality, and thus performance of the part can be affected by the overall present defects and their distribution throughout the structure. The study from Papon and Haque (2019) explored the functional relationship between fibre content and fracture properties (stress intensity factor or energy release rate) of the additively manufactured short fibre reinforced PLA composites produced by fused filament fabrication (FFF) based technique through compact tension (CT) testing (Papon and Haque, 2019). The use of a square-shaped nozzle to print the samples resulted in enhanced fracture toughness due to the lesser presence of inter-bead voids and larger bonded areas in comparison with those printed using a circular-shaped nozzle. They also reported that the fracture toughness of the CT specimens printed in the (0/90)° orientation has much higher percentage increase in comparison to those printed in (-45/45)° orientation.

As additive manufactured parts are built of layers of laminated strings, delamination is a typical structural damage resulting in the fracture of the component. Delamination is a crack that forms between adjacent plies and primarily occurs due to interlaminar stresses caused by structural and material discontinuities (Sridharan, 2008) (Heidari-Rarani et al., 2019), e.g. between two layers of different orientation or thicknesses. Once initiated, the crack could grow under constant loading or cyclic movement, reducing the load-bearing capabilities and stiffness of the component. It is therefore of critical importance to be able to characterise delamination.

When an applied load increases, the stored strain energy is released to initiate crack growth. As a result, the strain energy would change with the crack length. These strain energy differences will result in the dissipation of energy to increase the surface area of a crack. Through testing additively manufactured Acrylonitrile Butadiene-styrene (ABS) samples, Hart and Wetzel (2017) showed that the critical elastic/plastic strain energy release rate required to propagate cracks across the laminae was

approximately an order of magnitude greater than energy required to propagate cracks between laminae (Hart and Wetzel, 2017).

The Strain Energy Release Rate (SERR) associated with loading and boundary conditions irrespective of the specimen is the available strain energy, G. The available strain energy is a complex function of layer/laminate properties, thickness, layering sequence, as well as defect size, geometry and its location (Arteiro et al., 2020). SERR is an important factor when considering toughness of polymers (Kashtalyan and Soutis, 2006) (Syngellakis and Wu, 2008). The interlaminar fracture toughness can be described by the critical value of the strain energy release rate, G_C.

The relationship between the critical SERR, G_{IC} and fracture toughness, K_{IC} can be represented by Equation 1 (ASTM D5045-14, n.d.).

$$G_{IC} = \frac{(1-\nu^2)K_{Ic}^2}{E} \qquad \text{Equation 1}$$

where ν is Poisson's ratio and E is the Young's modulus.

If $G < G_c$, the existing crack will remain stable in its stationary state. To further extend the crack, the applied load must be increased. A stable crack growth will be achieved when $G = G_c$, by releasing strain energy when a new crack surface is created. The crack growth becomes unstable when $G > G_c$, which leads to a rapid fracture of the component.

When investigating the geometrical effect such as specimen's thickness and width on the SERR and toughness, there are various published works (Hoffmann et al., 2018) (Furtado et al., 2020) (Kheirkhah Barzoki et al., 2018a) (Tsai and Chen, 2005). Huang (1994) demonstrated that the influence of width of the test specimens on the strain-energy release rate could be ignored only when the width was at least eight times larger than the laminate thickness. (Jia Yen Huang, 1994). The energy release rates were affected by the thickness of the laminate. Another paper reported on a decrease in the energy release rates with thickness for laminates stacked with similar sub-laminates (Kheirkhah Barzoki et al., 2018b) .

The research described in this paper investigates the fracture properties, G_{IC} and K_{Ic} of additively manufactured PLA thin parts by conducting a three-point flexural testing using sub-size Single-Edge Notched Beam (SENB) specimens in accordance to the ASTM D5045 Standard (ASTM D5045-14, n.d.) (Raheem, 2019). Subjecting the thin/sub-size specimens to flexural in-situ testing inside an X-Ray Tomography (XRT) chamber will help to characterize the delamination or damage within the specimen or in-between layers with respect to the loading and displacement from which the toughness of the PLA material can be derived. In addition, the Charpy V-notched (CVN) impact testing that was performed on sub-size specimens of a specific thickness will allow for a comparison of methodologies in determining the SERR and fracture toughness, in this case with the flexural testing methodology. Meanwhile, a scanning electron microscope (SEM) was utilised to investigate defects and features in between layers and within the specimens such as air gap, delamination, and local plasticity that could affect the additively manufactured PLA's toughness.

In the absence of the Charpy impact testing standard procedure for the sub-size plastic or polymer specimens, the approach for the CVN impact testing adapted that of brittle (linear elastic) materials/metals (ASTM D6110-18, n.d.) (ASTM D6110-18, n.d.) (Roberts et al., 1981) (Wallin, 1992) (Dahlberg et al., 1992).. Finite element simulations and analysis based on the flexural testing were performed for comparison and verification of the experimental results as well as the suitability of the methodologies in determining the damage tolerance of the sub-size/thin additively manufactured PLA parts.

2. Methodologies

2.1. Materials and the FDM Process Parameters

PLA was the selected material for this investigation which has a Young's modulus of E_1=1331.94MPa and E_2=1061.20MPa, a Poisson's ratio υ of 0.38, and a shear modulus G_{12} of 1187.08MPa (determined from the in-house tensile and flexural testing).

The Three-point flexural and CVN impact testing were conducted following guidance in the ASTM D5045 (ASTM D5045-14, n.d.) and ASTM 6110 (ASTM D6110-18, n.d.), respectively. The thin and sub-size SENB and CVN test specimens were manufactured implementing the FDM technique using a Prusa MK2.5S printer (Figure 1). The FDM printing parameters are outlined in Table 1. The flexural test specimens were produced in two layer orientations of (0/90)° and (-45/45)° and three different thicknesses of 800μm, 1200μm and 1600μm. A sharp notch was manually produced by scalpel incision to a size that satisfied the plane strain fracture toughness conditions of $0.45 \leq a/W \leq 0.55$ where a is the notch length and W is the width of the sample (ASTM D5045-14, n.d.).

2.2. Three-point flexural Experimental Testing

The Three-point flexural test was conducted by applying mode I quasi-static loading with 0.1mm/min loading rate inside a test chamber of an X-Ray Tomography (XRT) Zeiss Xradia Versa 520. The test rig for the determination of the flexural properties according to BS EN ISO 178 (ISO 178:2010, n.d.) and ASTM D790 (ASTM D790 - 17, n.d.) has been scaled down by a factor of five to fit into the machine. Figure 2 shows the rig arrangement inside the XRT.

The determination of the G_{IC} and K_{Ic} followed the ASTM 5045 procedure, Annex 1 (ASTM D5045-14, n.d.). G_{IC} and K_{Ic} were evaluated using their conditional values notated as G_Q and K_Q respectively for the bend specimen following the validity requirements and the solutions given in ASTM 5045.

G_Q is calculated using the following equations:

$$G_Q = \frac{U}{BW\varphi} \qquad \text{Equation 2}$$

where: U is the corrected energy, B and W are the thickness and width of the test specimens respectively, whilst the energy calibration factor, φ was computed from the Equation 3.

$$\varphi = \frac{A+18.64}{dA/dx} \qquad \text{Equation 3}$$

The polynomial solutions for the *A* and *dA/dx* (mathematical variables in Equation 3) are as follows:

$$A = [16x^2/(1-x)^2] [8.9 – 33.717x +79.616 x^2 – 112.952x^3 + 84.815x^4 – 25.672x^5]$$

$$dA/dx = [16x^2/(1-x)^2] [-33.717+159.232x – 338.856x^2 + 339.26x^3 – 128.36x^4] + [32x/(1-x)^3] [8.9 – 33.717x +79.616 x^2 – 112.952x^3 + 84.815x^4 – 25.672x^5]$$

$x = a/W$; where a is the crack length after fracture.

Meanwhile, K_Q is calculated using Equation 4 for the $0 < x < 1$ condition given in the standard.

$$K_Q = \left(\frac{P_Q}{B.W^{1/2}}\right) f(x) \qquad \text{Equation 4}$$

where: P_Q is the load and;

$$f(x) = 6x^{1/2} \frac{[1.99 - x(1-x)(2.15 - 3.93x + 2.7x^2)]}{(1+2x)(1-x)^{3/2}}$$

2.3. Three-point flexural Finite Element Modelling and Simulation

A finite element method available via the commercial package ABAQUS CAE 2019 was used to analyse the strain elastic energy due to the brittle nature of PLA. The bending process was simulated with a symmetrical system. PLA material properties and FDM process parameters as presented in Table 1 in the “Materials ” section were used and these modelled specimen were then bent in the middle with a cylinder which had a radius, *R* of 1mm. The support on the plate was fixed in the vertical direction (y-direction); while, the symmetrical outline of the model was fixed along the z-direction as depicted with the wireframe model in Figure 3. The cross-section was fixed in the longitudinal direction (x-direction) with the crack area set to be free. Figure 3 also illustrates an example of the ABAQUS model with its mesh. The quarter of the cylinder was modelled as a discrete rigid body using C3D8R linear element with a mesh size parameter of 0.1. A reference point was applied to control the bending process through a defined displacement. The C3D8R linear element with mesh size of 0.1 was also applied for the plate (specimen) model. The surface-to-surface contact between the rigid part and the plate (specimen) was set with a friction coefficient of 0.3.

The stress intensity factor, *K* with a maximum energy release rate was chosen as the ABAQUS output of the FE simulation. In the plane stress condition, the strain energy release rate G_{IC} can be determined using Equation 1 in relation to the K_{IC}-values and the PLA properties.

2.4. Charpy V-Notch (CVN) Impact Testing

The CVN impact test method determines the amount of energy absorbed by a material during fracture to describe the toughness or impact strength of the material in the presence of a flaw or notch and fast loading conditions. The energy absorbed would be a function of both the elastic and plastic deformation within the specimen at the onset and growth of the crack from the notch root. Such a process is also sensitive to stress state and therefore the size of the specimen. The CVN Impact testing gives an estimation of the minimum fracture toughness needed for a fracture to occur. During the test, a swinging pendulum fractures the notched specimen and the remaining energy of the pendulum is measured.

In this work, a miniaturised FDM printed specimen was subjected to the CVN impact test. The implication of using a miniaturised specimen would be in the reduction of the constraints for plane strain conditions, thus in the absorbed energy to fracture the specimen per unit volume and therefore promotes brittle failure.

The sub-size CVN specimens of 3000μm were manufactured using the same FDM parameters outlined in Table 1 with the geometry and dimension shown in Figure 4. A 5 Joule maximum Charpy Impact test machine was utilised.

The correlations between the CVN energy and K_{IC} for a sub-size brittle plastic specimen were adapted the lower shelf-lower bound formula of Roberts and Newton (Roberts et al., 1981) as well as of INSTA (Dahlberg et al., 1992) to determine the additively manufactured PLA fracture toughness.

The correlation formula of Roberts and Newton (Roberts et al., 1981) is represented in Equation 5:

$$K_{Ic} = 0.804 \cdot \sigma_{ys} \cdot (\frac{CVN}{\sigma_{ys}} - 0.0098)^{0,5} \qquad \text{Equation 5}$$

where CVN is the energy absorbed by the specimen and σ_{ys} is the material's yield strength. A normalisation factor NF is introduced:

$$NF = \frac{CVN}{SSC} \approx \frac{0,521}{0,5} \approx 10 \qquad \text{Equation 6}$$

where SSC is the absorbed energy of the sub-sized Charpy impact test specimen that allows for the correlation between the sub-sized CVN and the standard-sized test specimens.

Alternatively, K_{IC} can be correlated to the CVN energy (in Joule) using a standard but more conservative solution as shown in Equation 7 (Dahlberg et al., 1992) .

$$K_{IC} = 12\sqrt{CVN} \qquad \text{Equation 7}$$

The relation between the SERR and the fracture toughness is shown in Equation 1.

3. Results and Discussion

As 3D prints are highly dependent on process parameters, visual examination is the recommended first step to reduce the number of misprints and to allow a consistent quality of a printed part. Defects such as stringing or a coarse surface due to a faulty extrusion by a clogged nozzle are easy to notice. The refinement of the process parameters requires a lot of fine-tuning of the printer settings to result in a reduction of these defects. When the parts are printed with brims to allow a higher stability whilst printing, some of the brims will remain after the removal on the specimen (Figure 5). These remains can be carefully removed for the most part by simply using a fresh razor blade or sharp scalpel.

Air gaps between the filament strings are also noticeable when printing the first layers of a part. These air gaps are formed in a rectilinear pattern of the print setting and their size will depend on the diameter of the circular nozzle used. An extensive fine-tuning of the system was conducted to minimise these air gaps. The average air gap's longest length for (0/90)° and (-45/45)° specimens when using a $400\mu m$ diameter nozzle was 61μm and 140μm respectively. The raster of the 100% infill specimens with a raster orientation of (0/90)° was wider than that of those specimens with raster orientation of (-45/45)°, leaving less space for the air gaps.

The Scanning Electron Microscope (SEM) images of a fractured specimen revealed that some of these air gaps that were formed between filament strings had been extended in the direction of loading. Later cracks, as shown in Figures 6 and 7 from the XRT, were seen to initiate and grow from these air gaps as loading was applied. In addition, delamination between layers was also observed.

It has been known that delamination forms during the testing between adjacent plies which primarily occurs due to interlaminar stresses caused by structural and material discontinuities (Sridharan, 2008) (Sankarabatla, n.d.) (Pozuelo et al., 2006). In this experiment, it was observed that the delamination mostly started from the tip of the air gaps, separating the two layers of different orientation.

The quality of the interfaces between the layers would determine the number of delaminated layers which could be used as an indicator for the laminated toughness. This is aligned with the energy release rate, *G* definition which is the rate at which the energy is transformed for a material to undergo fracture (i.e. onset and growth). As the number of delaminated layers increases, the impact energy absorbed by a specimen will rise (Pozuelo et al., 2006). The interlaminar fracture toughness can therefore be described by the critical value of the strain energy release rate G_C.

Table 2 and Figures 8 and 9 represent the in-situ flexural testing results from which G_Q and K_Q were determined. From the results it can be seen that the coefficient of variation (*CV*) which is a relative standard deviation indicates a low-variance for all the geometries (when $CV \leq 1$). The experimental results are also compared with the toughness values derived from the FEA, as represented in Figures 10 and 11. Within those figures, the referenced values for both G_{IC} and K_{IC} of solid (moulded) PLA are included. The published data of G_{IC} was estimated to be between 2.4 kJ/m^2 and 6.5

kJ/m^2 (Nascimento et al., 2010) (Park et al., 2004) and of K_{IC} to be between 2.87 – 3.37 MPa√m (Tagarielli et al., 2017) .

The flexural test results reveal that the toughness values of the specimens are influenced by the layer orientation and the number of layers or the thickness of the specimen. Larger number of layers or thicker specimens causes higher values of SERR and fracture toughness. These are true for all outcomes obtained from both the experiments and FEA. The FEA considered only the elastic strain energy and did not consider the onset and growth or deformation ahead of the air gap voids and the delamination in the modelling and simulation. The FEA results therefore showed lower G_{IC} and K_{IC} values for all the specimens than the experimental ones. However, they are only marginally different in values (up to 10%). This is mainly associated with the specimens' main mode of fracture which is indicative of a mode I intra-laminar fracture, as shown by the Optical Microscope (OM) and Scanning Electron Microscope (SEM) images of the specimens (Figures 12-15). For the specimens printed in the (0/90)º orientation, the fracture surface observations characterised a brittle cleavage failure with relatively smooth and planar matrix fracture, demonstrated by the mode I fracture surface. For the (-45/45) º test specimens, the tension side of the surface (Figure 16) showed that the fracture path was angled at approximately 45º, a typical representation of a shear crack.

Meanwhile, the K_{IC} results of the as-printed CVN impact test specimens are presented in Table 3. These values were derived using the conversion of impact energy (Joule) solutions given in Equations 5 (Roberts et al., 1981) and 7 (Dahlberg et al., 1992) . The Robert and Newton's (R&N) solution that incorporated a normalisation factor for the sub-size specimen showed in relatively lower value than the standard solution (applied to a standard 25mm specimen). In general, these thicker as-printed specimens of 3000μm resulted in lower fracture toughness than the flexural testing. The specimens revealed brittle fractures (Figure 17). The 5 Joule impact energy used in the impact testing clearly surpassed the energy absorbed that is required for forming and growing the cracks and to delaminate. In other words, the approach did not allow for these local events to be taken into account in the toughness evaluation.

4. Conclusion

The critical SERR (G_{IC}) and fracture toughness (K_{IC}) of the additively manufactured PLA sub-size specimens were determined from the flexural and the CVN impact testing experiment. The energy approach as per the ASTM 5045 provided a reasonable method to determine both the G_{IC} and K_{IC} of a sub-size specimen. This method would be more preferable than the CVN impact testing method.

The additively manufactured PLA's toughness and its fracture behaviour were strongly influenced by the FDM process parameters and specimen geometries, such as nozzle diameter, temperature, speed, layer orientation, raster as well as the specimen's thickness. One of the impacts on the choice of nozzle and raster sizes discussed was on the air gaps formation and delamination between layers. The XRT confirmed that the onset and growth of the crack occurred at the tip of the rectilinear shaped air gaps. The local energy adsorbed to grow the crack/fracture and to delaminate contributed to the increase in the toughness of the materials. This contributes to the higher toughness values of the flexural test specimens than those derived from the Finite Element analysis and from the CVN impact test. Subsequently, all specimens demonstrated the mode I intra-laminar fracture behaviour.

The following are the summary of the results:

- The (-45/45)° specimens showed relatively higher toughness values than the (0/90)° specimens which were derived experimentally and numerically.
- A higher toughness value was obtained for the larger number of layers or thicker flexural specimens.
- For thicker CVN impact test specimens, relatively lower toughness values than those of the flexural specimens were determined.
- The methodology is sensitive to the stress state of the specimen.
- The CVN impact test method could not sensitively capture the effect of an increase in the energy absorbed for the air gaps to plastically deform and for delamination to take place.
- ASTM 5045's energy approach provides a viable method to determine toughness of a sub-size specimen.

References

Arteiro, A., Furtado, C., Catalanotti, G., Linde, P., Camanho, P.P., 2020. Thin-ply polymer composite materials: A review. Compos. Part Appl. Sci. Manuf. 132, 105777. https://doi.org/10.1016/j.compositesa.2020.105777

ASTM D790 - 17, n.d. ASTM D790 - 17 Standard Test Methods for Flexural Properties of Unreinforced and Reinforced Plastics and Electrical Insulating Materials.

ASTM D790 : Standard Test Methods for Flexural Properties of Unreinforced and Reinforced Plastics and Electrical Insulating Materials [WWW Document], n.d.

ASTM D5045-14, n.d. Test Methods for Plane-Strain Fracture Toughness and Strain Energy Release Rate of Plastic Materials. ASTM International. https://doi.org/10.1520/D5045-14

ASTM D6110-18, n.d. ASTM D6110-18 - Standard Test Method for Determining the Charpy Impact Resistance of Notched Specimens of Plastics.

Auras, R., Harte, B., Selke, S., 2004. An Overview of Polylactides as Packaging Materials. Macromol. Biosci. 4, 835–864. https://doi.org/10.1002/mabi.200400043

Chin Ang, K., Fai Leong, K., Kai Chua, C., Chandrasekaran, M., 2006. Investigation of the mechanical properties and porosity relationships in fused deposition modelling-fabricated porous structures. Rapid Prototyp. J. 12, 100–105. https://doi.org/10.1108/13552540610652447

Dahlberg, L., Andreasen, W., Bergman, M., Dellby, O., Knudsen, T., Lindewald, C.-G., Naess, O.J., Niemi, E., Wallin, K., 1992. Assessment of the integrity of structures containing discontinuities.

Diegel, O., 2014. 10.02 - Additive Manufacturing: An Overview, in: Hashmi, S., Batalha, G.F., Van Tyne, C.J., Yilbas, B. (Eds.), Comprehensive Materials Processing. Elsevier, Oxford, pp. 3–18. https://doi.org/10.1016/B978-0-08-096532-1.01000-1

Farah, S., Anderson, D.G., Langer, R., 2016. Physical and mechanical properties of PLA, and their functions in widespread applications — A comprehensive review. Adv. Drug Deliv. Rev. 107, 367–392. https://doi.org/10.1016/j.addr.2016.06.012

Furtado, C., Arteiro, A., Linde, P., Wardle, B.L., Camanho, P.P., 2020. Is there a ply thickness effect on the mode I intralaminar fracture toughness of composite laminates? Theor. Appl. Fract. Mech. 107, 102473. https://doi.org/10.1016/j.tafmec.2020.102473

Guo, N., Leu, M.C., 2013. Additive manufacturing: technology, applications and research needs. Front. Mech. Eng. 8, 215–243. https://doi.org/10.1007/s11465-013-0248-8

Hart, K.R., Wetzel, E.D., 2017. Fracture behavior of additively manufactured acrylonitrile butadiene styrene (ABS) materials. Eng. Fract. Mech. 177, 1–13. https://doi.org/10.1016/j.engfracmech.2017.03.028

Heidari-Rarani, M., Rafiee-Afarani, M., Zahedi, A.M., 2019. Mechanical characterization of FDM 3D printing of continuous carbon fiber reinforced PLA composites. Compos. Part B Eng. 175, 107147. https://doi.org/10.1016/j.compositesb.2019.107147

Hoffmann, J., Cui, H., Petrinic, N., 2018. Determination of the strain-energy release rate of a composite laminate under high-rate tensile deformation in fibre direction. Compos. Sci. Technol. 164, 110–119. https://doi.org/10.1016/j.compscitech.2018.05.034

ISO 178:2010, n.d. ISO 178:2010, Plastics — Determination of flexural properties.

Jia Yen Huang, 1994. Studies of geometry effects on strain-energy release rate of composite laminate. Eng. Fract. Mech. 47, 893–900. https://doi.org/10.1016/0013-7944(94)90067-1

Kalita, S.J., 2010. 13 - Rapid prototyping in biomedical engineering: structural intricacies of biological materials, in: Sharma, C.P. (Ed.), Biointegration of Medical Implant Materials, Woodhead Publishing Series in Biomaterials. Woodhead Publishing, pp. 349–397. https://doi.org/10.1533/9781845699802.3.349

Kashtalyan, M., Soutis, C., 2006. Modelling off-axis ply matrix cracking in continuous fibre-reinforced polymer matrix composite laminates. J. Mater. Sci. 41, 6789–6799. https://doi.org/10.1007/s10853-006-0207-4

Kheirkhah Barzoki, P., Rezadoust, A.M., Latifi, M., Saghafi, H., 2018a. The experimental and numerical study on the effect of PVB nanofiber mat thickness on interlaminar fracture toughness of glass/phenolic composites. Eng. Fract. Mech. 194, 145–153. https://doi.org/10.1016/j.engfracmech.2018.03.027

Kheirkhah Barzoki, P., Rezadoust, A.M., Latifi, M., Saghafi, H., 2018b. The experimental and numerical study on the effect of PVB nanofiber mat thickness on interlaminar fracture toughness of glass/phenolic composites. Eng. Fract. Mech. 194, 145–153. https://doi.org/10.1016/j.engfracmech.2018.03.027

Lanzotti, A., Grasso, M., Staiano, G., Martorelli, M., 2015. The impact of process parameters on mechanical properties of parts fabricated in PLA with an open-source 3-D printer. Rapid Prototyp. J. 21, 604–617. https://doi.org/10.1108/RPJ-09-2014-0135

Murphy, S.V., Atala, A., 2014. 3D bioprinting of tissues and organs. Nat. Biotechnol. 32, 773–785. https://doi.org/10.1038/nbt.2958

Nascimento, L., Gamez-Perez, J., Santana, O.O., Velasco, J.I., Maspoch, M.L., Franco-Urquiza, E., 2010. Effect of the Recycling and Annealing on the Mechanical and Fracture Properties of Poly(Lactic Acid). J. Polym. Environ. 18.

Papon, E.A., Haque, A., 2019. Fracture toughness of additively manufactured carbon fiber reinforced composites. Addit. Manuf. 26, 41–52. https://doi.org/10.1016/j.addma.2018.12.010

Park, S.-D., Todo, M., Arakawa, K., 2004. Effect of annealing on the fracture toughness of poly(lactic acid). J. Mater. Sci. 39, 1113–1116. https://doi.org/10.1023/B:JMSC.0000012957.02434.1e

Petrovic, V., Gonzalez, J.V.H., Ferrando, O.J., Gordillo, J.D., Puchades, J.R.B., Griñan, L.P., 2011. Additive layered manufacturing: sectors of industrial application shown through case studies. Int. J. Prod. Res. 49, 1061–1079. https://doi.org/10.1080/00207540903479786

Pozuelo, M., Carreño, F., Ruano, O.A., 2006. Delamination effect on the impact toughness of an ultrahigh carbon–mild steel laminate composite. Compos. Sci. Technol. 66, 2671–2676. https://doi.org/10.1016/j.compscitech.2006.03.018

Raheem, Z., 2019. Standard Test Methods for Plane-Strain Fracture Toughness and Strain Energy Release Rate of Plastic Materials 1. https://doi.org/10.1520/D5045-14

Roberts, R., Newton, C., Welding Research Council, 1981. Interpretive report on small-scale test correlations with KIC data. Welding Research Council, New York.

Sankarabatla, V.N.R., n.d. EFFECTS OF STRAIN ENERGY RELEASE RATE ON DELAMINATION IN TEMPERATURE ENVIRONMENT 81.

Singh, R., Singh, S., Hashmi, M.S.J., 2016. Implant Materials and Their Processing Technologies, in: Reference Module in Materials Science and Materials Engineering. Elsevier. https://doi.org/10.1016/B978-0-12-803581-8.04156-4

Sood, A.K., Ohdar, R.K., Mahapatra, S.S., n.d. Parametric appraisal of mechanical property of fused deposition modelling processed parts. Mater. Amp Des. 31, 287–295.

Sridharan, S., 2008. Delamination Behaviour of Composites. Elsevier.

Syngellakis, S., Wu, J., 2008. Evaluation of polymer fracture parameters by the boundary element method. Eng. Fract. Mech. 75, 1251–1265. https://doi.org/10.1016/j.engfracmech.2007.04.009

Tagarielli, V., Song, Y., Li, Y., Song, W., Yee, K., Lee, K.Y., 2017. Measurements of the mechanical response of unidirectional 3D-printed PLA. 164. https://doi.org/10.1016/j.matdes.2017.03.051

Tsai, G.-C., Chen, J.-W., 2005. Effect of stitching on Mode I strain energy release rate. Compos. Struct. 69, 1–9. https://doi.org/10.1016/j.compstruct.2004.02.009

Wallin, K., 1992. Guidelines for deriving fracture toughness estimates from normal and miniature size Charpy-V specimen data. J. Struct. Mech. 25, 24–40.

Zhang, Q., Zhang, K., Hu, G., 2016. Smart three-dimensional lightweight structure triggered from a thin composite sheet via 3D printing technique. Sci. Rep. 6, 1–8. https://doi.org/10.1038/srep22431

Figures

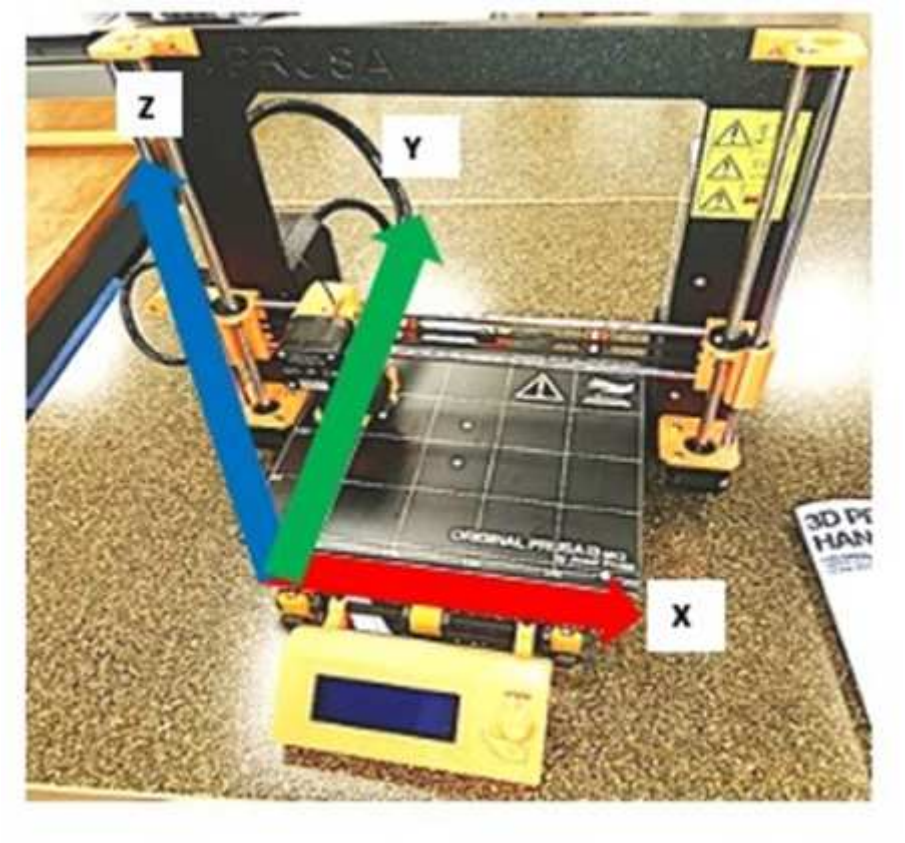

Figure 1

FDM Printer and the reference coordinate system for printing

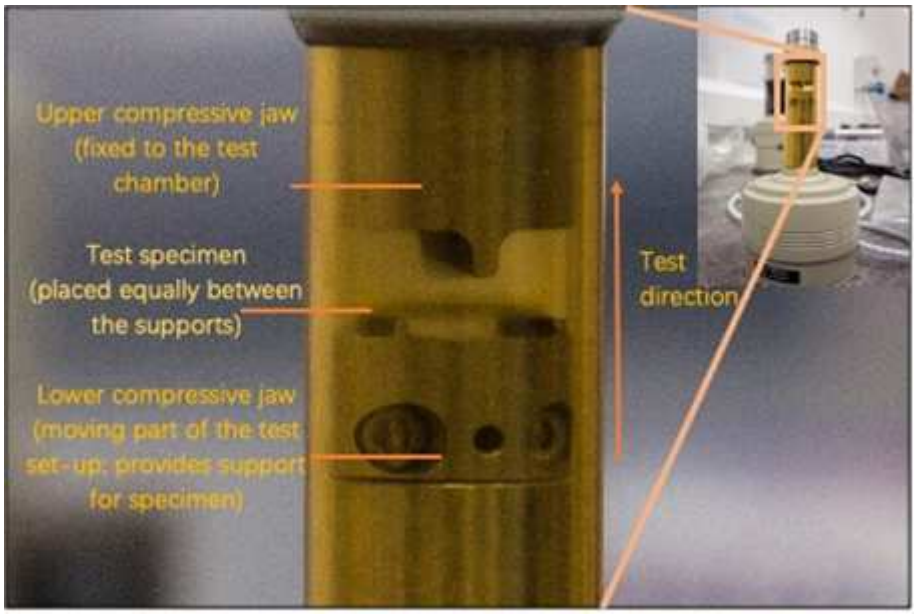

Figure 2

The flexural test rig arrangement inside the XRT chamber

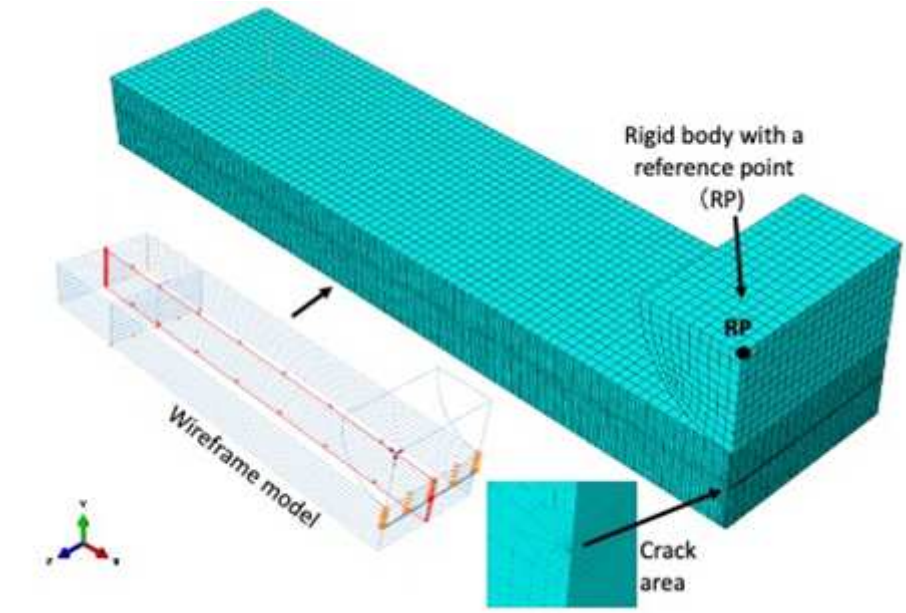

Figure 3

3D model and meshing arrangement for symmetric bending

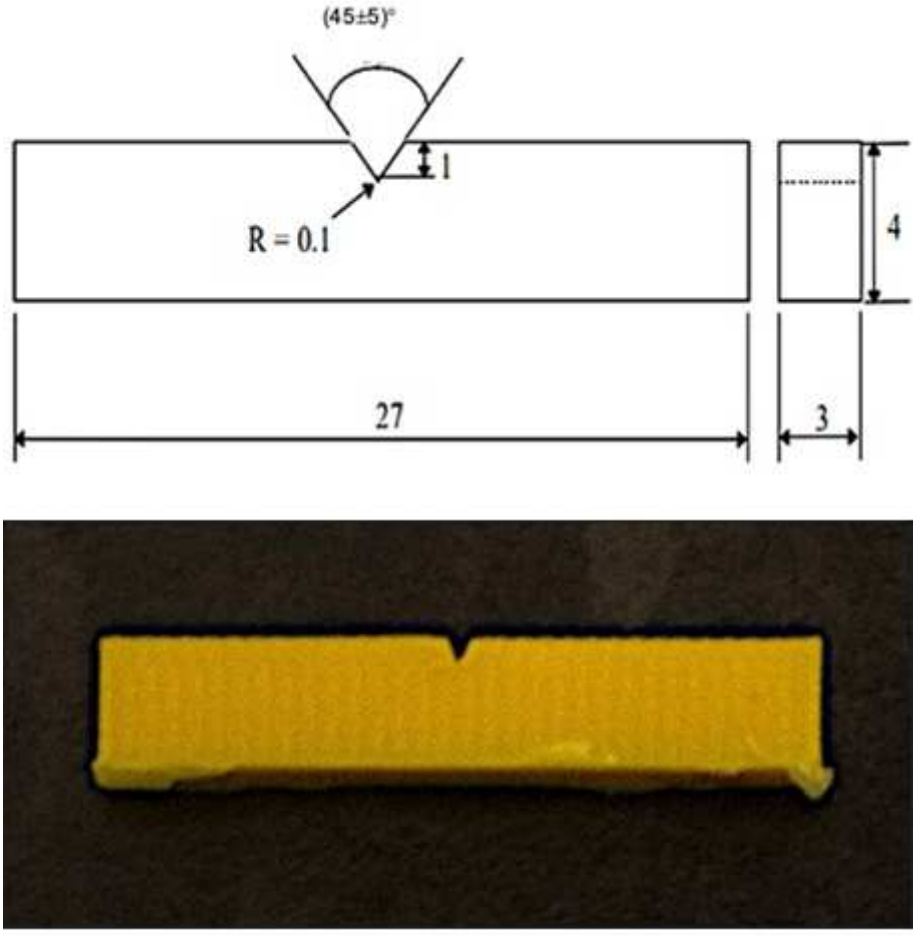

Figure 4

(a) A sketch and (b) printed sub-size CVN sample (dimension: 27 X 4 X 3, all in mm)

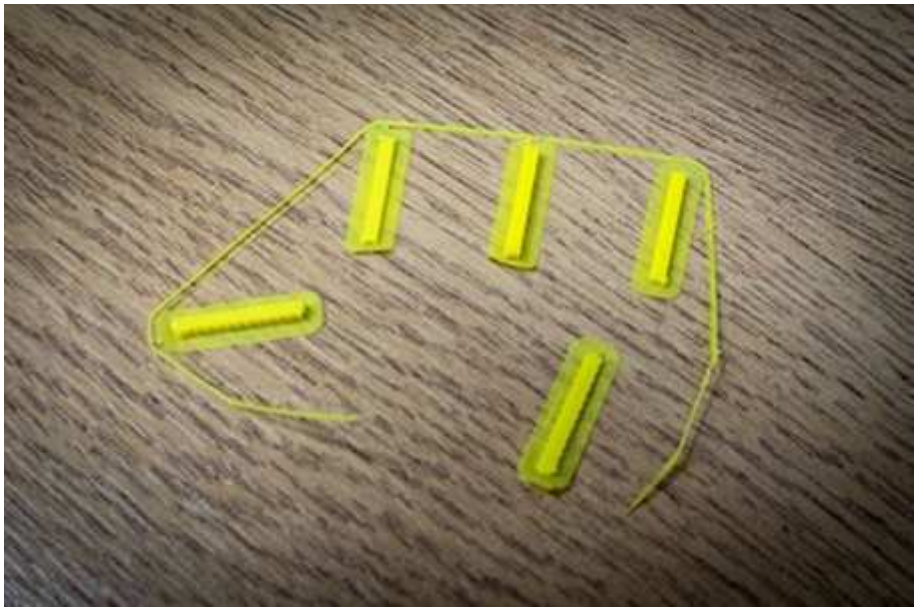

Figure 5

AM flexural specimens with attached brims

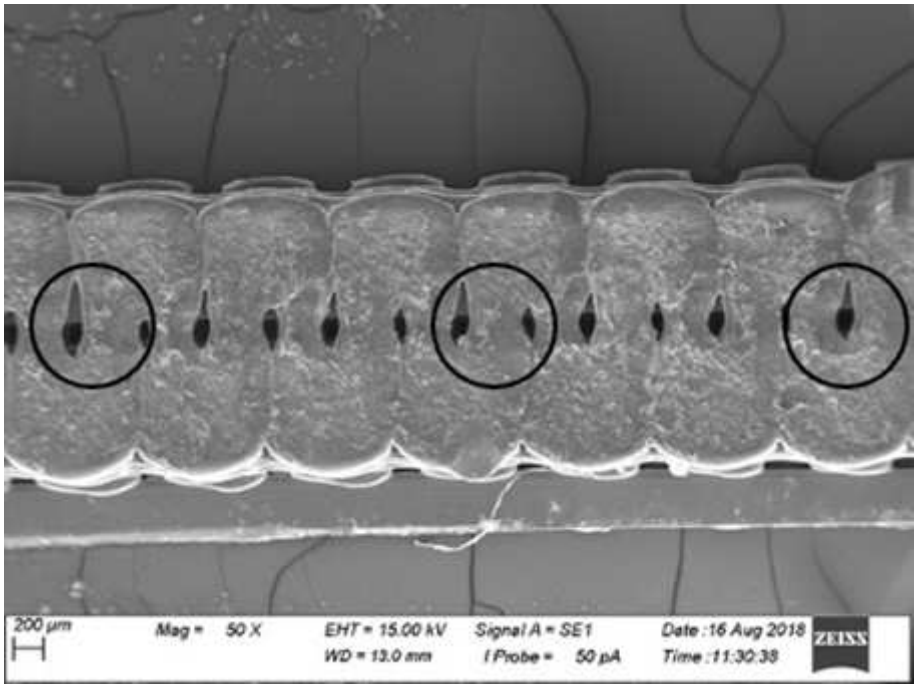

Figure 6

Flexural test fractured specimens showing the air gaps between filament strings using a 400µm diameter nozzle, some extended (examples highlighted in circles) and grew as cracks when loading

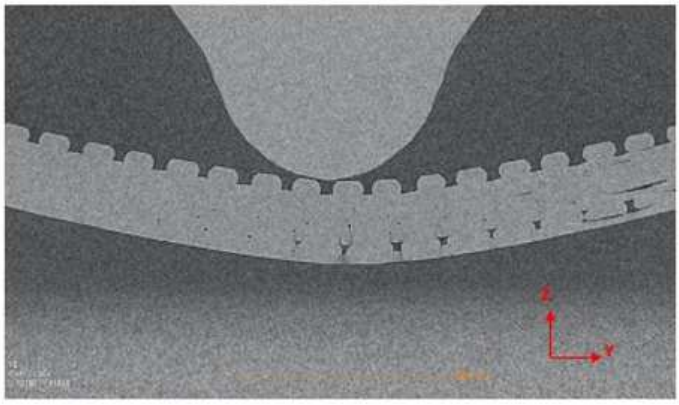

(a)

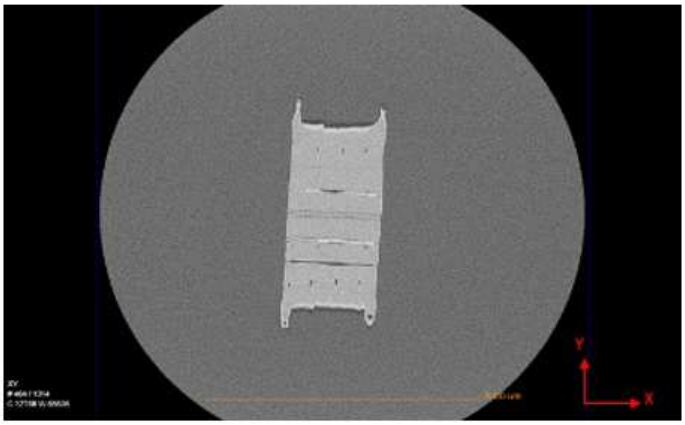

(b)

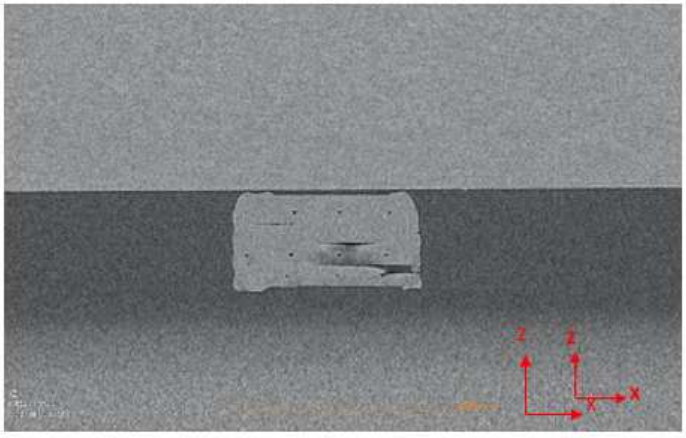

(c)

Figure 7

The XRT in-situ flexural 8 layered test sample in (a) YZ, (b) XY and (c) XZ orientation

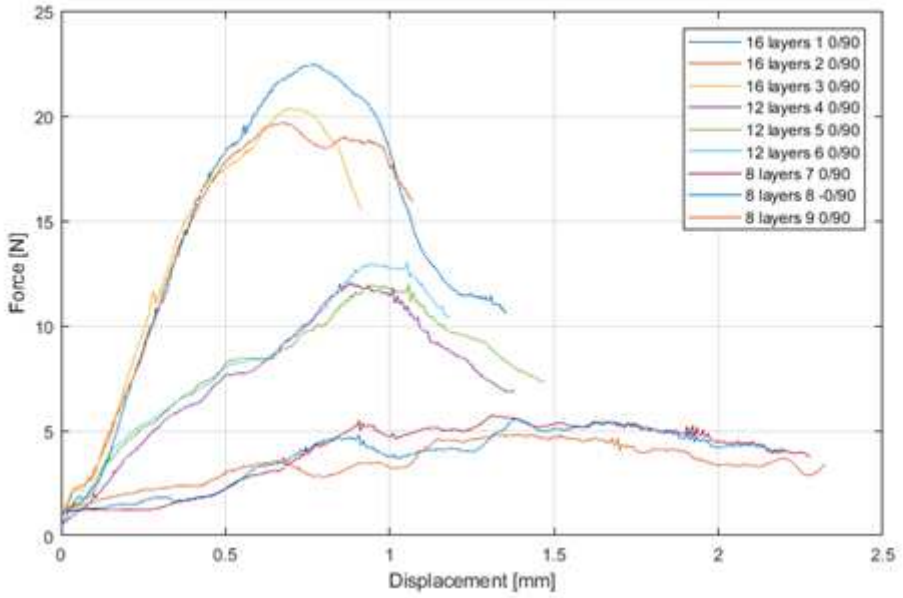

Figure 8

Force vs displacement curves for specimens printed in (0/90)° orientation

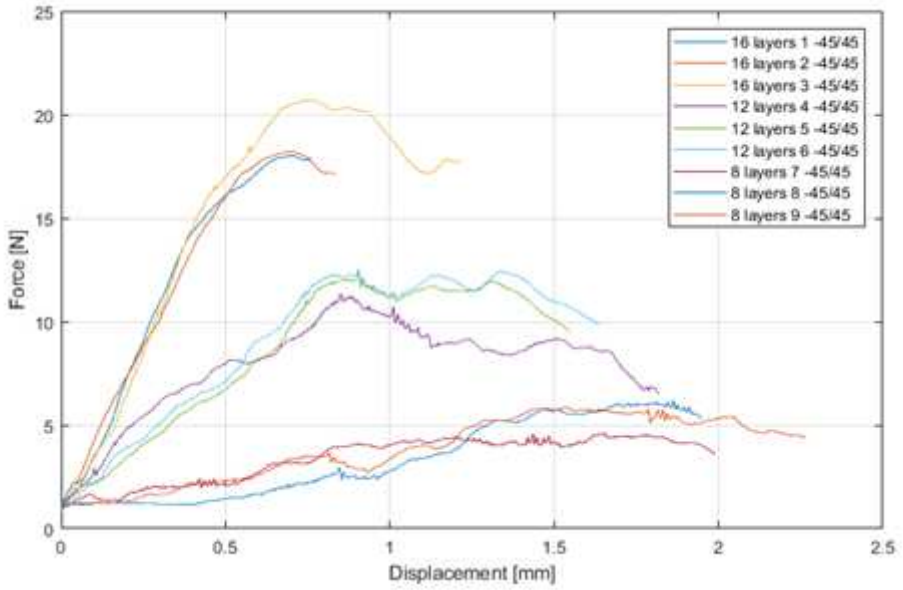

Figure 9

Force vs displacement curves for specimens printed in (-45/45)° orientation

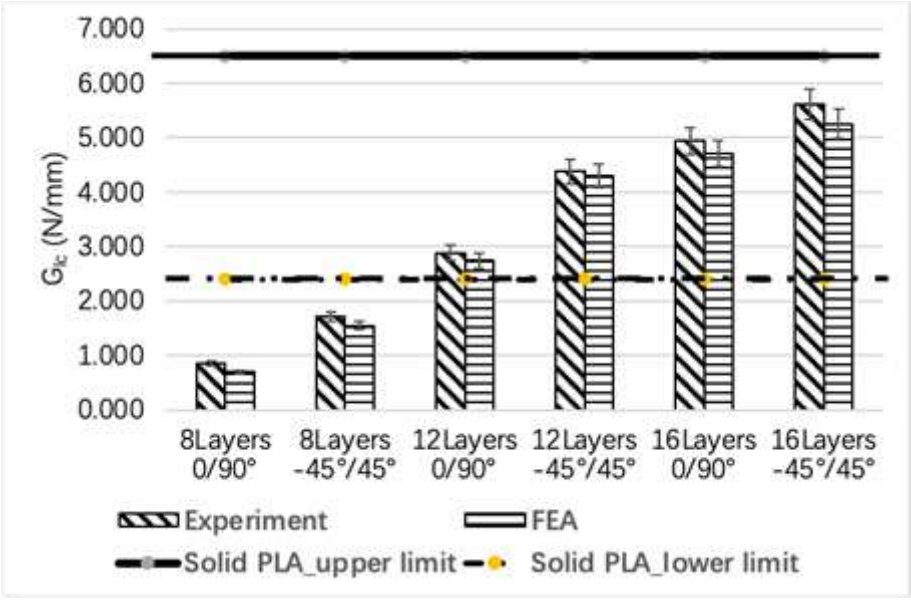

Figure 10

GIC experimental vs. FEA values

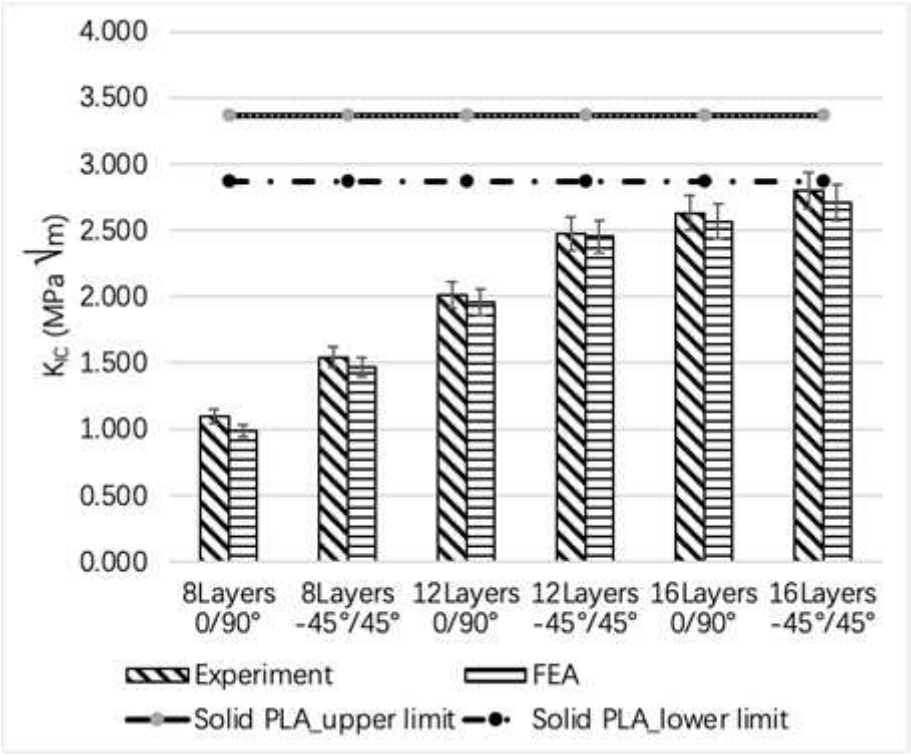

Figure 11

KIC experimental vs. FEA values

Figure 12

OM image showing a mode I fracture (highlighted in red circle) in the (0/90)° orientation, 8-layer printed specimen

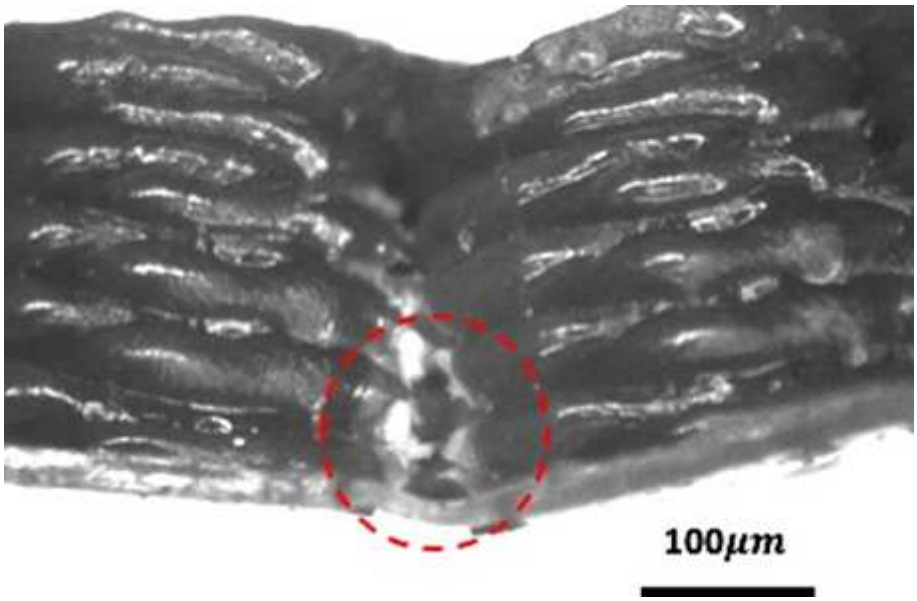

Figure 13

OM image showing a mode I fracture (highlighted in red circle) in the (-45/45)° orientation, 12-layer printed specimen

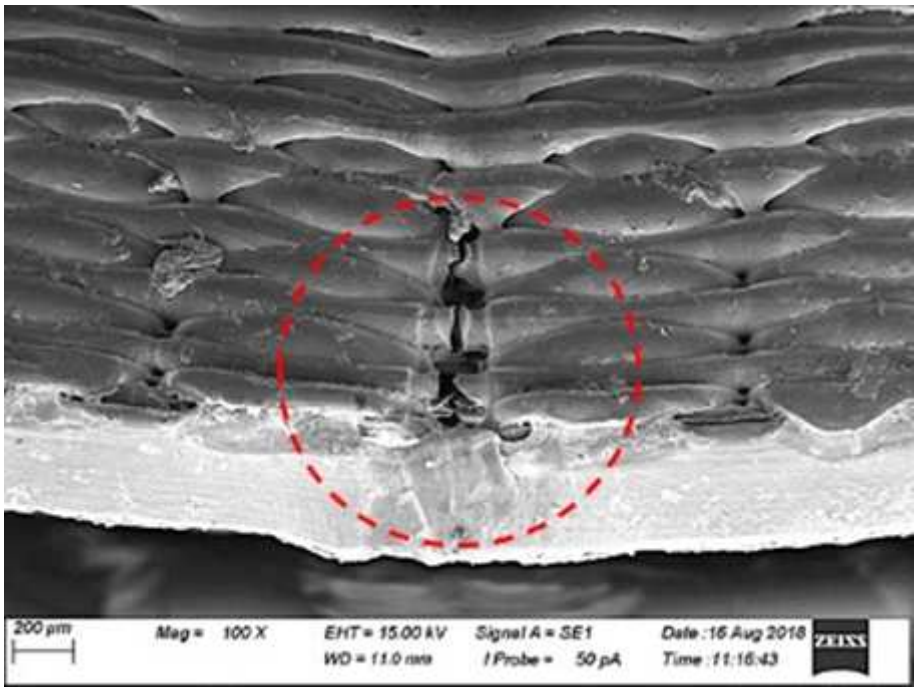

Figure 14

SEM image showing a mode I fracture (highlighted in red circle) in (0/90)° orientation, 16-layer printed specimen

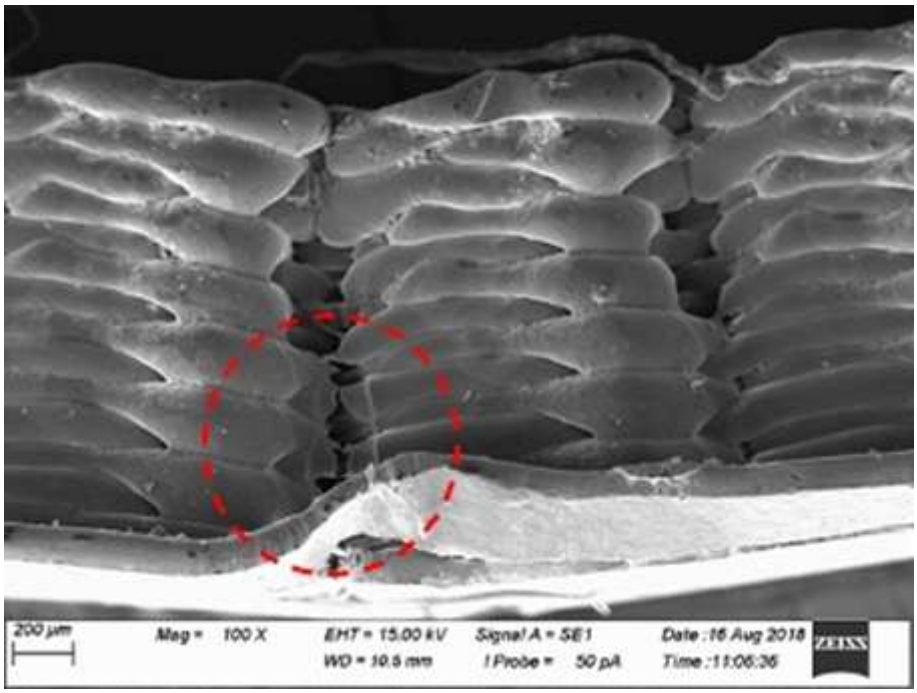

Figure 15

SEM image showing a mode I fracture (highlighted in red circle) in (-45/45)° orientation, 16-layer printed specimen

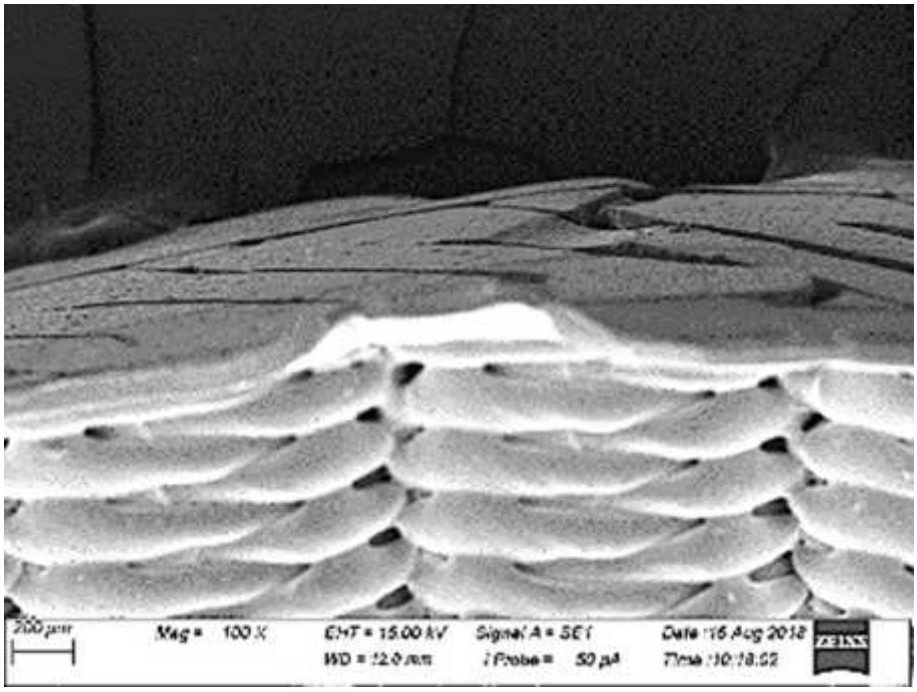

Figure 16

SEM image showing surface fracture of a 12-layer printed specimen in (-45/45)° orientation

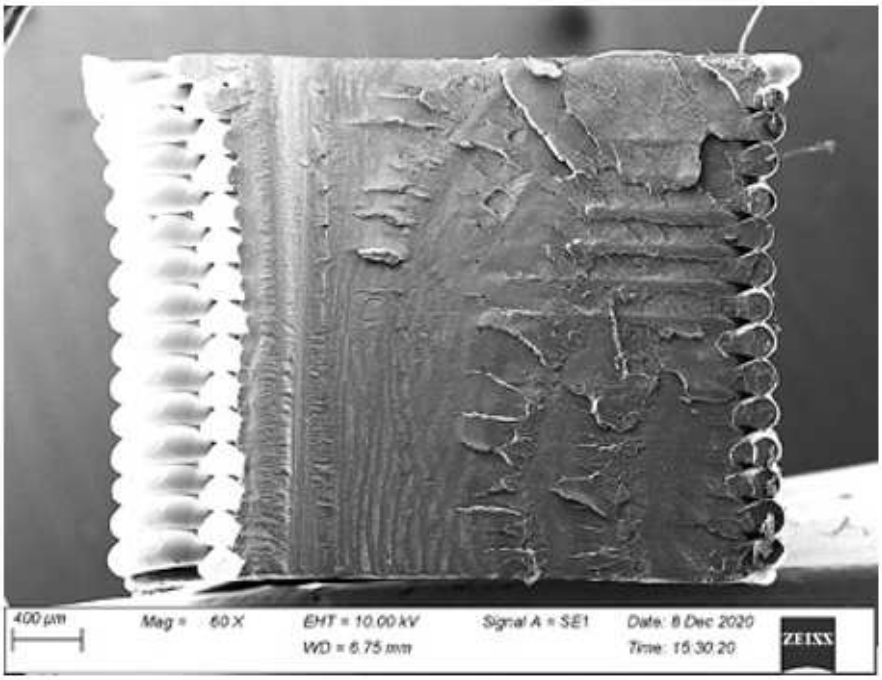

(a)

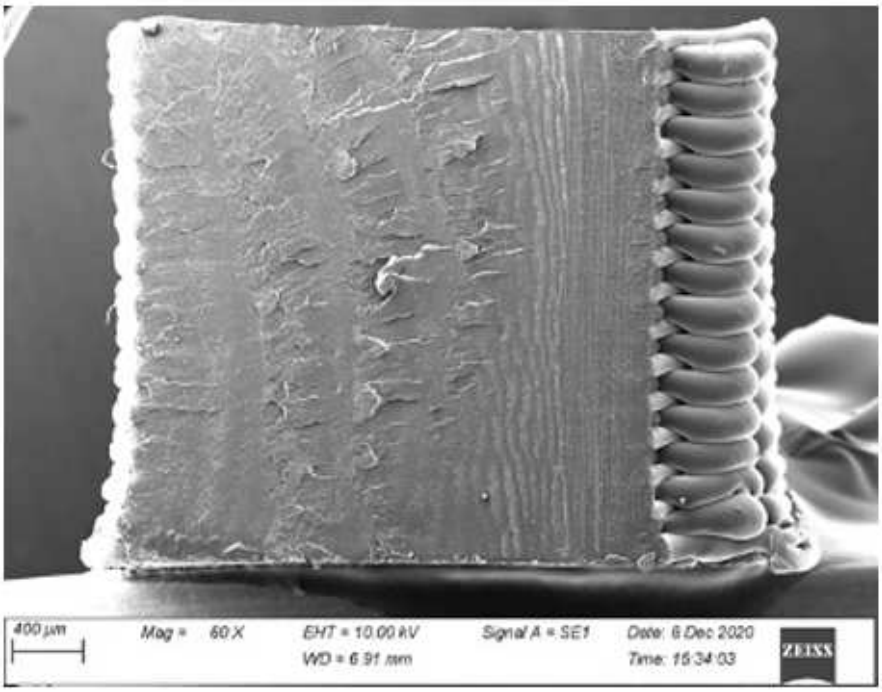

(b)

Figure 17

SEM images showing the CVN impact test specimens surface fracture of the (0/90)° and (b) (-45/45)° orientations